

Rotational enhancement and stability of protoquark stars during thermal evolution

Adamu Issifu  ^{1, 2, *} Andreas Konstantinou  ^{3, 4, †} Prashant Thakur  ^{5, ‡} and Tobias Frederico  ^{1, 2, §}

¹*Departamento de Física, Instituto Tecnológico de Aeronáutica,
DCTA, 12228-900, São José dos Campos, SP, Brazil*

²*Laboratório de Computação Científica Avançada e Modelamento (Lab-CCAM), Brazil*

³*Department of Physics, University of Cyprus, P.O. Box 20537, 1678 Nicosia, Cyprus*

⁴*Computation-based Science and Technology Research Center,
The Cyprus Institute, 20 Kavafi Str., Nicosia 2121, Cyprus*

⁵*Department of Physics, Yonsei University, Seoul, 03722, South Korea*

We present the first systematic study of rigidly rotating protoquark stars based on isentropic equations of state (EOS) within the density-dependent quark mass (DDQM) framework. Using a quasi-static equilibrium approach, we follow the Kelvin–Helmholtz evolution from hot, lepton-rich matter to a cold, catalyzed quark star. Rotation substantially enhances the maximum stable mass (by up to $\sim 40\%$), equatorial radius, and key rotational observables, with the ratio of rotational kinetic to gravitational potential energy, $T_{\text{kin}}/|W|$, reaching 0.18–0.19 near the Keplerian limit, indicating a heightened susceptibility to gravitational-wave-emitting instabilities. Thermal evolution introduces a clear ordering: all stellar properties peak during the lepton-rich stages and decrease monotonically as the star cools. Compared to hadronic stars, rotating protoquark stars exhibit larger radii, higher moments of inertia, and stronger quadrupolar deformation, producing a distinct signature in the mass–radius–spin plane that can accommodate objects such as HESS J1731–347 and PSR J0740+6620. These results demonstrate that future multimesenger observations must account for both thermal history and rotation to robustly identify quark matter in compact stars.

I. INTRODUCTION

The theoretical possibility of compact objects composed of self-bound up (u), down (d), and strange (s) quarks has attracted long-standing interest in nuclear astrophysics [1, 2]. The existence of such objects is motivated by the conjecture that strange quark matter may constitute the true ground state of nuclear matter [3–5]. On this basis, several studies have speculated that some observed pulsars, including Her X-1, the X-ray burster 4U 1820–30, HESS J1731–347, and XTE J1810–197, could be interpreted as quark stars [6–9]. A definitive identification of compact objects, however, requires establishing a consistent connection between their internal composition and macroscopic structure through confrontation with observational data. In particular, rotational observables, such as the spin frequency, angular momentum, and moment of inertia, provide key diagnostics for distinguishing quark stars from hadronic configurations. Early studies of rotating quark stars can be found in Refs. [10–14].

Early studies of rotating strange stars, based on simplified EOS that neglected quark masses and interactions, predicted Keplerian frequencies comparable to or even lower than those of neutron stars [10, 15, 16], reflecting their relatively low maximum masses. In contrast, modern EOS incorporating quark masses and interactions, including those adopted here, support substantially higher maximum masses and correspondingly larger rotational frequencies [17, 18]. Consequently, the rotational

properties of self-bound quark stars differ qualitatively from those of neutron stars. Uniform rotation can increase the maximum mass of a quark star by more than 40% [17, 19, 20], compared with a typical $\sim 20\%$ enhancement for neutron stars, while differential rotation can sustain even more massive configurations [21–23]. Moreover, the ratio of rotational kinetic to gravitational binding energy, $T_{\text{kin}}/|W|$, is significantly larger for quark stars [17, 19], indicating an enhanced susceptibility to non-axisymmetric instabilities, although triaxial deformation may ultimately limit their attainable spin rates [24, 25].

In this work, we study the rotational properties of protoquark stars within a quasi-static approximation, in which the thermodynamic conditions, such as the entropy per baryon s_B and the lepton fraction Y_l , are fixed at each evolutionary stage. Rotating equilibrium configurations are constructed using the open-source `rns` code [26]. The underlying EOS is modeled within the DDQM framework, with parameters selected from Table II of [27] in order to maximize the stellar mass. The thermodynamics of hot quark matter follows the formalism introduced in Sec. II B of [28], which focuses on static protoquark stars. The evolution is represented by a sequence of equilibrium snapshots corresponding to four distinct stages. Within this framework, we compute the mass–radius relation, the distribution of the core temperature along stellar sequences, and several key rotational observables. These include the mass as a function of spin frequency, the moment of inertia, angular momentum, polar redshift, and quadrupole moment as functions of the stellar mass. A central result of this study is the complete energy decomposition of rotating protoquark stars, which provides complementary information of direct relevance for observational missions [29].

To our knowledge, this work presents the first systematic investigation of rotating protoquark stars based

* ai@academico.ufpb.br

† akonst29@ucy.ac.cy

‡ prashant@yonsei.ac.kr

§ tobias@ita.br

on isentropic EOS. Earlier studies of rotating hot compact quark stars employing isothermal EOS can be found in [30]. The possible role of strange quark matter in the early universe has also been explored in [31]. A full general relativistic simulation of rapidly rotating quark stars, including oscillation modes and universal relations, can also be found in [32].

This paper is organized as follows. In section II, we introduce the model formalism and the equation of state, which is discussed in detail in section II.1 and separated into the cold (section II.1.1) and hot (section II.1.2) quark matter sectors. The formalism used to describe the rotational properties is presented in section II.2. The results and their analysis are given in section III, and our conclusions are summarized in section IV.

II. MODEL DESCRIPTION AND FORMALISM

II.1. The equation of state

The presentation of the EOS is divided into two parts to fully investigate the star's evolutionary process. We first discuss the cold, catalyzed quark matter configuration, followed by the finite-temperature protoquark star phase. The EOS that forms the foundation of this study is derived from [28], where the effective temperature was introduced through a phenomenological method. The appropriate coupling constants were also adopted from [27], in which the authors determined the free model parameters of the DDQM using Bayesian inference in light of recent astrophysical data.

II.1.1. Cold quark matter

The quark matter (QM) EOS is described using the density-dependent quark mass (DDQM) approach. In this framework, the interaction among quarks is encoded through the baryon density ρ_B , which determines how the quark masses vary with the medium. The density dependence is introduced via the ansatz [33, 34]:

$$m_i = m_{i0} + \frac{D}{\rho_B^{1/3}} + C \rho_B^{1/3}, \quad (1)$$

where m_{i0} ($i = u, d, s$) denotes the current quark masses and C and D are model parameters. Although widely used, the DDQM model is known to violate thermodynamic consistency. A standard remedy is to replace the free chemical potential μ_i with an effective one, μ_i^* , which explicitly depends on ρ_B , and to employ the density-dependent quark masses $m_i(\rho_B)$ in the thermodynamic potential. The free-energy density is then expressed as

$$f = \Omega_0(\{\mu_i^*\}, \{m_i\}) + \sum_i \mu_i^* n_i, \quad (2)$$

where the thermodynamic potential takes the form (see [28] and references therein)

$$\Omega_0 = - \sum_i \frac{\gamma_i}{24\pi^2} \left[\mu_i^* \nu_i \left(\nu_i^2 - \frac{3}{2} m_i^2 \right) + \frac{3}{2} m_i^4 \ln \left(\frac{\mu_i^* + \nu_i}{m_i} \right) \right], \quad (3)$$

with $\gamma_i = 6$ accounting for spin and color degeneracy. The corresponding Fermi momentum is

$$\nu_i = \sqrt{\mu_i^{*2} - m_i^2}, \quad (4)$$

leading to the number density

$$\rho_i = \frac{\gamma_i}{6\pi^2} (\mu_i^{*2} - m_i^2)^{3/2} = \frac{\gamma_i \nu_i^3}{6\pi^2}. \quad (5)$$

The physical chemical potential is related to its effective counterpart through

$$\mu_i = \mu_i^* - \mu_I, \quad (6)$$

where μ_I encodes the interaction shift. Under β -equilibrium, the chemical potentials satisfy

$$\mu_u^* + \mu_e = \mu_d^* = \mu_s^*. \quad (7)$$

The construction of the EOS further requires a global charge neutrality,

$$\frac{2}{3} \rho_u - \frac{1}{3} \rho_d - \frac{1}{3} \rho_s - \rho_e = 0, \quad (8)$$

and baryon number conservation,

$$\rho_B = \frac{1}{3} (\rho_u + \rho_d + \rho_s). \quad (9)$$

The energy density follows from

$$\varepsilon = \Omega_0 - \sum_i \mu_i^* \frac{\partial \Omega_0}{\partial \mu_i^*}, \quad (10)$$

while the pressure is obtained from

$$p = -\Omega_0 + \sum_{i,j} \frac{\partial \Omega_0}{\partial m_j} \rho_i \frac{\partial m_j}{\partial \rho_i}. \quad (11)$$

II.1.2. Hot Quark Matter

We begin with the temperature-dependent free energy density f , which serves as the foundation for deriving the energy density ε and pressure p through a self-consistent thermodynamic framework expressed in terms of the temperature T . Hence,

$$\begin{aligned} f &= f(T, V, \{\rho_i\}, \{m_i\}) \\ &= \Omega_0(T, V, \{\mu_i^*\}, \{m_i\}) + \sum_{i=u,d,s} \mu_i^* \rho_i, \end{aligned} \quad (12)$$

where V is the volume of the system. Since the independent state variables do not include the μ_i^* appearing in

Ω_0 , we must establish a link between μ_i^* and the independent variables. This connection is introduced through the particle number density ρ_i :

$$\rho_i = -\frac{\partial}{\partial \mu_i^*} \Omega_0(T, V, \{\mu_i^*\}, \{m_i\}). \quad (13)$$

Taking the derivative of Eq. (12) we have

$$df = d\Omega_0 + \sum_i \rho_i d\mu_i^* + \sum_i \mu_i^* d\rho_i, \quad (14)$$

with

$$d\Omega_0 = \frac{\partial \Omega_0}{\partial T} dT + \sum_i \frac{\partial \Omega_0}{\partial \mu_i^*} d\mu_i^* + \sum_i \frac{\partial \Omega_0}{\partial m_i} dm_i + \frac{\partial \Omega_0}{\partial V} dV, \quad (15)$$

and

$$dm_i = \frac{\partial m_i}{\partial T} dT + \sum_j \frac{\partial m_i}{\partial \rho_j} d\rho_j. \quad (16)$$

Substituting Eqs. (15) and (16) into Eq. (14) and grouping the terms, we have

$$df = \left(\frac{\partial \Omega_0}{\partial T} + \sum_i \frac{\partial \Omega_0}{\partial m_i} \frac{\partial m_i}{\partial T} \right) dT + \sum_i \left(\mu_i^* + \sum_j \frac{\partial \Omega_0}{\partial m_j} \frac{\partial m_j}{\partial \rho_i} \right) d\rho_i + \frac{\partial \Omega_0}{\partial V} dV. \quad (17)$$

Comparing the above expression with the thermodynamic relation

$$df = -SdT + \sum_i \mu_i d\rho_i + \left(-P - f + \sum_i \mu_i \rho_i \right) \frac{dV}{V}, \quad (18)$$

we can express the entropy S as:

$$S = -\frac{\partial \Omega_0}{\partial T} - \sum_i \frac{\partial m_i}{\partial T} \frac{\partial \Omega_0}{\partial m_i}, \quad (19)$$

the pressure as:

$$p = -f + \sum_i \mu_i \rho_i - V \frac{\partial \Omega_0}{\partial V}, \quad (20)$$

and the chemical potential in terms of the effective chemical potential is given explicitly as:

$$\mu_i = \mu_i^* + \sum_j \frac{\partial \Omega_0}{\partial m_j} \frac{\partial m_j}{\partial \rho_i} \equiv \mu_i^* - \mu_I. \quad (21)$$

The last term in Eq. (20) persists when the finite size effect of the system cannot be neglected, whether the particle masses are fixed or not. However, it can be ignored in this study just like other previous studies of DDQM [33, 35–37], considering an infinitely large system of QM. In this case, the free energy density is independent of V , and

substituting Eqs. (12) and (21) into Eq. (20), the pressure becomes

$$p = -\Omega_0 + \sum_{i,j} \rho_i \frac{\partial \Omega_0}{\partial m_j} \frac{\partial m_j}{\partial \rho_i}. \quad (22)$$

The energy density is determined by substituting Eqs. (12) and (19) into $f = \varepsilon - TS$, yielding

$$\varepsilon = \Omega_0 + \sum_i \mu_i^* \rho_i - T \frac{\partial \Omega_0}{\partial T} - T \sum_i \frac{\partial m_i}{\partial T} \frac{\partial \Omega_0}{\partial m_i}. \quad (23)$$

For a given independent variables T and ρ_i , the μ_i^* are found by solving Eq. (13). All thermodynamic quantities follow from Eqs. (19), (21), (22), and (23). The finite-temperature extension of the quark mass formula is

$$m_i = m_{i0} + \frac{D}{\rho_B^{1/3}} \left(1 + \frac{8T}{\Lambda} e^{-\Lambda/T} \right)^{-1} + C \rho_B^{1/3} \left(1 + \frac{8T}{\Lambda} e^{-\Lambda/T} \right), \quad (24)$$

with $\Lambda = 280$ MeV [38], $C = 0.8$, and $\sqrt{D} = 127.4$ MeV [27]. These parameters are deliberately chosen to yield the maximum possible stable quark star mass within the optimized parameter space identified in [27]. As shown there, decreasing C or increasing \sqrt{D} relative to the values adopted here results in a smaller maximum stable quark star mass. The current quark masses follow PDG values: $m_u = 2.16$ MeV, $m_d = 4.67$ MeV, $m_s = 93.4$ MeV [39]. This temperature-dependent quark mass relation has been adopted in [28, 35, 40]. The qualitative interpretation of the T -dependence in Eq. (24) is associated with thermal screening effects in the quark-gluon medium. As the temperature increases, the same thermal factor,

$$f(T) = 1 + \frac{8T}{\Lambda} e^{-\Lambda/T}, \quad (25)$$

encoding the excitation of quark-antiquark pairs and gluons oppositely modulates the two ρ_B -dependent contributions: it enhances the repulsive term proportional to $\rho_B^{1/3}$, increasing the effective quark mass at high densities and stiffening the DDQM EOS through a larger pressure contribution, while suppressing the confining term proportional to $\rho_B^{-1/3}$, thereby screening the color interaction and driving the system toward asymptotic freedom.

II.2. Rotational Properties

In this work, rigidly rotating protoquark stars are modeled using the `rns` code [26]. The code solves Einstein's field equations for a stationary and axisymmetric space-time, described by the line element

$$ds^2 = -e^{\gamma+\lambda} dt^2 + e^{2\alpha} (dr^2 + r^2 d\theta^2) + e^{\gamma-\lambda} r^2 \sin^2 \theta (d\phi - \omega dt)^2, \quad (26)$$

where the metric potentials γ, λ, α , and ω depend on the radial coordinate r and the polar angle θ . The global stellar quantities, including the gravitational mass M , baryonic mass M_0 , angular momentum J , equatorial circumferential radius R_e , and polar redshift Z_p , are computed following Eqs. (B1), (B2), (B4), (B6), and (B7) of Ref. [41], respectively. The moment of inertia is defined as $I = J/\Omega$, where $\Omega = 2\pi\nu$ is the angular velocity and ν the spin frequency. The rotational kinetic energy is given by

$$T_{\text{kin}} = \frac{J\Omega}{2}, \quad (27)$$

while the binding energy is defined as

$$E_{\text{bind}} = M - M_0. \quad (28)$$

The gravitational potential energy is evaluated as

$$|W| = |M_p + T_{\text{kin}} - M|, \quad (29)$$

where the proper mass M_p is defined according to Eq. (65) of Ref. [42]. The internal energy is then obtained as

$$U = M_p - M_0. \quad (30)$$

The mass quadrupole moment is determined from the asymptotic expansion of the metric functions at large distances. Within the **rns** framework, the coefficient M_2 is extracted from the $r^{-3}P_2(\cos\theta)$ term in the expansion of the ρ -potential [43, 44]. The physical quadrupole moment Q is then obtained as

$$Q = M_2 - \frac{4}{3} \left(\frac{1}{4} + b \right) M^3, \quad (31)$$

where b is a dimensionless coefficient determined from the asymptotic behavior of the metric potentials (see Eq. (9) of Ref. [43]), and M_2 corresponds to the $l = 2$ multipole coefficient of the expansion [44]. We compute the percentage (%) increase in maximum mass enhancement using the relation:

$$\Delta M_{\text{max}}(\%) = \frac{M_{\text{max}}(r_p/r_e) - M_{\text{max}}(1.0)}{M_{\text{max}}(1.0)} \times 100. \quad (32)$$

III. RESULTS AND ANALYSIS

Table I summarizes the properties of rotating protoquark stars at their maximum mass across four evolutionary stages and demonstrates that rotation and thermal history, in an isentropic scenario, jointly govern their global structure. Increasing rotation (decreasing r_p/r_e) systematically raises the maximum mass (M), equatorial radius (R_e), angular momentum (J), moment of inertia (I), and quadrupole moment (Q), while the ratio $T_{\text{kin}}/|W|$ increases to $\sim 0.18\text{--}0.19$ near the Keplerian limit (ν_K), indicating strong centrifugal support. The spin frequency (ν) peaks for the most oblate configurations, and centrifugal flattening leads to enhanced I and quadrupole

deformations. Along the M sequence, the polar redshift Z_p also increases; the increase in mass and decrease in polar radius r_p together outweigh the centrifugal weakening of the gravitational potential.

At fixed rotation, thermal evolution introduces a clear and systematic ordering: as the star deleptonizes from hot, lepton-rich to cold, catalyzed states, the M decreases slightly, R_e contracts, and the J , I , and Q all decline as the star becomes more compact. The temperature T at a fixed mass of $2.0 M_\odot$ shows two competing effects: it decreases with increasing rotation (rotational cooling), but increases with s_B during deleptonization before vanishing in the cold, catalyzed limit. In contrast, the ν at M rises with cooling, since a colder, stiffer EOS allows faster rotation before mass shedding, while $T_{\text{kin}}/|W|$ remains primarily determined by the degree of flattening rather than temperature.

The relative increase in the M_{max} , grows monotonically with rotation and reaches values of up to $\sim 40\%$ at the Kepler limit for hot, lepton-rich configurations. This enhancement exceeds the typical $\sim 20\%$ found for hadronic stars [14, 19, 23] and is consistent with universal relations predicting $\sim 15\text{--}20\%$ for hadronic matter [45] and $\sim 20\text{--}33\%$ for self-bound quark stars [46]. A direct comparison with Ref. [47], which studied rotating stars composed of nucleonic, hyperonic, and Δ -baryon matter, shows that purely nucleonic EOS yield a $\sim 9\text{--}13\%$ increase at the Keplerian limit, while the inclusion of Δ -isobars leads to enhancements of up to $\sim 21\%$.

The large values of $T_{\text{kin}}/|W|$ attained near the ν_K ($\sim 0.18\text{--}0.19$) indicate that rapidly rotating protoquark stars are susceptible to the Chandrasekhar–Friedman–Schutz secular instability, which can drive sustained gravitational-wave emission from non-axisymmetric modes [48]. The softer EOS and enhanced equatorial expansion of quark matter allow these stars to reach higher $T_{\text{kin}}/|W|$ than their hadronic counterparts, strengthening their prospects as detectable sources of continuous gravitational waves from young compact remnants [49, 50]. Astrophysically, these trends imply that rapidly rotating, hot protoquark stars can support very large masses and develop strong quadrupole deformations, making them promising gravitational-wave sources and potentially long-lived against collapse. They further highlight that mass, radius, spin, redshift, and gravitational-wave information must be combined to reliably infer the underlying EOS and thermal state, as rotation and temperature effects can otherwise mask the true nature of the stellar interior.

The gravitational mass–equatorial radius sequences shown in fig. 1 demonstrate how finite-temperature effects and rotation govern the structural evolution of protoquark stars, with hot, lepton-rich configurations exhibiting larger radii than the cold, catalyzed limit. Similar trends were found for nonrotating protoquark stars in [28, 56]. This behavior contrasts with purely hadronic protoneutron stars, which are more compact and support lower maximum masses in the lepton-rich phase, then expand and reach higher maximum masses during the hotter, higher-entropy and lepton-poor deleptonization stage, before

TABLE I. Stellar properties at maximum mass for different quasi-static evolutionary stages of rotating protoquark stars parameterized by r_p/r_e . The angular momentum J , moment of inertia I , quadrupole moment $|Q|$, radius R , gravitational redshift Z_p , the ratio of the rotational kinetic energy T_{kin} to the gravitational potential energy $|W|$, and the spin frequency ν are determined at the maximum mass M_{max} . Also shown are the stellar radius at $1.4 M_\odot$, $R_{1.4}$, and the temperature at $2.0 M_\odot$, $T_{2.0}$ (this is deliberately chosen to amplify the variation of T with r_p/r_e , the variations at M_{max} can be found in fig. 2).

Model	r_p/r_e	M_{max}	R	$R_{1.4}$	J	I	$ Q $	$T_{2.0}$	ΔM_{max}	Z_p	$T_{\text{kin}}/ W $	ν
		$[M_\odot]$	[km]	[km]	$[10^{49} \text{ gcm}^2 \text{s}^{-1}]$	$[10^{45} \text{ gcm}^2]$	$[10^{42} \text{ gcm}^2]$	[MeV]	[%]			[Hz]
$s_B = 1, Y_l = 0.4$	1.0	2.33	14.71	14.92	0.00	—	0.00	9.43	0.0	0.38	0.00	0.00
	0.9	2.45	15.39	15.52	1.79	4.95	202.49	8.90	5.2	0.42	0.03	577.08
	0.8	2.59	16.40	16.21	2.93	5.90	474.62	8.31	11.2	0.47	0.07	789.94
	0.7	2.79	17.82	17.04	4.29	7.47	899.78	7.67	19.7	0.53	0.12	913.96
	0.6	3.03	19.73	18.08	6.02	9.79	1554.55	6.98	30.0	0.59	0.15	977.73
	0.5	3.27	22.33	19.37	7.93	12.63	2417.96	6.23	40.3	0.63	0.19	999.93
$s_B = 2, Y_l = 0.2$	1.0	2.28	14.44	14.72	0.00	—	0.00	20.32	0.0	0.38	0.00	0.00
	0.9	2.39	15.17	15.32	1.71	4.67	189.73	19.07	4.8	0.41	0.03	582.23
	0.8	2.54	16.09	16.02	2.81	5.55	447.74	17.71	11.4	0.46	0.07	804.74
	0.7	2.72	17.25	16.67	4.07	6.77	805.63	16.27	19.3	0.52	0.11	956.54
	0.6	2.96	19.09	17.55	5.70	8.83	1383.42	14.78	29.8	0.59	0.15	1027.09
	0.5	3.20	21.89	—	7.55	11.77	2246.61	—	40.4	0.62	0.18	1021.57
$s_B = 2, Y_{\nu_e} = 0$	1.0	2.24	14.26	14.68	0.00	—	0.00	22.53	0.0	0.37	0.00	0.00
	0.9	2.35	14.98	15.27	1.65	4.44	182.64	21.07	4.9	0.41	0.03	590.25
	0.8	2.49	15.88	15.97	2.70	5.27	426.80	20.06	11.2	0.46	0.07	814.72
	0.7	2.67	17.11	16.82	3.92	6.50	776.60	18.15	19.2	0.52	0.10	959.49
	0.6	2.90	18.89	17.88	5.46	8.40	1315.96	16.60	29.5	0.58	0.14	1035.26
	0.5	3.12	21.70	19.24	7.18	11.15	2123.04	14.93	39.3	0.61	0.18	1024.37
$T = 0$	1.0	2.20	14.03	14.50	0.00	—	0.00	—	0.0	0.37	0.00	0.00
	0.9	2.30	14.70	15.10	1.58	4.17	170.56	—	4.5	0.41	0.03	602.17
	0.8	2.44	15.65	15.80	2.59	5.01	405.79	—	10.9	0.46	0.07	824.24
	0.7	2.62	16.86	16.65	3.77	6.17	737.89	—	19.1	0.51	0.10	970.70
	0.6	2.84	18.57	17.71	5.24	7.92	1238.79	—	29.1	0.58	0.14	1052.82
	0.5	3.05	21.33	18.99	6.86	10.47	1984.78	—	38.6	0.61	0.18	1043.31

contracting again in the cold limit [57–59]. The contrast reflects the underlying microphysics: hadronic matter stiffens during deleptonization due to thermal pressure and repulsive nuclear interactions, whereas quark matter is already thermally inflated at early times and contracts monotonically as thermal support is removed during cooling.

As rotation increases, quantified by a decreasing polar-to-equatorial radius ratio r_p/r_e , centrifugal support enlarges the equatorial radius and raises the maximum gravitational mass, as indicated by the star symbols along each sequence. The most oblate configurations ($r_p/r_e \approx 0.5$) approach the Keplerian limit (see fig. 3). This qualitative behavior is consistent with that of hadronic stars [47] (and references therein); however, for uniform rotation, quark stars are expected to enhance their maximum mass by up to $\sim 40\%$ [14, 19], compared to $\sim 20\%$ for hadronic stars, with even larger increases anticipated for differential rotation [22, 23], where the angular velocity varies with position. This is attributed to quark matter's softer high-density response and larger equatorial expansion under rotation. Consequently, rapidly rotating protoquark stars occupy a distinct region of the mass–radius plane, where both the enlarged radius and the rotation-induced mass

enhancement must be accounted for when constraining the underlying EOS.

The agreement of the cold, catalyzed configurations with the HESS J1731–347 [60] and NICER PSR J0740+6620 [54] constraints reflects the ability of the QM EOS to remain stiff at high densities. In this limit, thermal and lepton pressures vanish, and the star is supported solely by the zero-temperature QM EOS, which simultaneously accommodates the low-mass, small-radius HESS object and the high-mass, moderate-radius PSR J0740+6620. Rotational support further shifts some sequences toward larger equatorial radii, allowing rapidly rotating cold configurations to overlap with the upper NICER contours. Together, these features show that a single QM model can explain the observed spread in the mass–radius plane and underscore the importance of rotation when interpreting cold-EOS constraints from multi-messenger data.

Figure 2 shows the core temperature as a function of gravitational mass for sequences of rotating protoquark stars. The main result is the substantial influence of rotation, parameterized by r_p/r_e , on both the thermal properties and the stability limits of these stars. For a fixed stellar mass, increased rotational flattening (lower

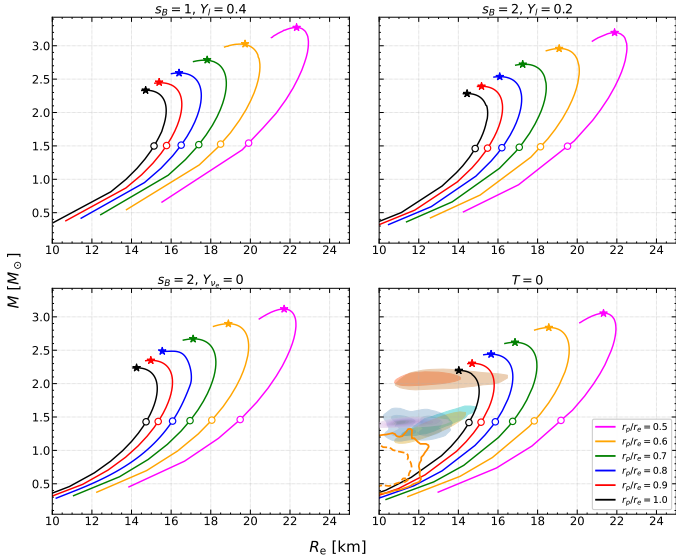


FIG. 1. The gravitational mass M of rotating protoquark stars as a function of equatorial radius R_e . In all four panels, the small circles along each curve represent the structural evolution of a single star with a fixed baryonic mass of $M_b = 1.55 M_\odot$. This serves as the baseline configuration, corresponding to $\sim 1.45 M_\odot$ cold, catalyzed neutron star. In other cases, this gravitational mass can differ depending on the conditions and can be clearly seen in the figure. In the $T = 0$ panel, we also have observational constraints, i.e. the steel blue area indicates the constraints obtained from the binary components of GW170817, with their respective 90% and 50% credible intervals. Additionally, the plot includes the 1σ (68%) CI for the 2D mass-radius posterior distributions of the millisecond pulsars PSR J0030 + 0451 (in cyan and yellow color) [51, 52] and PSR J0740 + 6620 (in orange and peru color) [53, 54], based on NICER X-ray observations. Furthermore, we display the latest NICER measurements for the mass and radius of PSR J0437-4715 [55] (lilac color). The supernova remnant HESS J1731-347 [7] is shown in red, with the outer contour representing the 90% CL and the inner contour representing the 50% CL.

r_p/r_e) reduces gravitational compression, resulting in systematically lower core temperatures along each sequence. The starred points indicate the maximum stable mass for each configuration, showing that rapid rotation significantly increases the mass threshold for gravitational collapse compared to the non-rotating case. Along the stable branch, the core temperature rises monotonically with gravitational mass due to increasing central compression, while beyond the maximum mass, the configurations become unstable and the temperature increases as the gravitational mass decreases, signaling a loss of hydrostatic support. The sequence of panels, from $s_B = 1, Y_l = 0.4$ characteristic of the immediate post-formation phase, to the states, $s = 2, Y_l = 0.2$ and $s = 2, Y_{\nu_e} = 0$, captures the star's evolution through deleptonization and neutrino transparent states. Together, these results map the thermodynamic trajectories accessible to hot, rotating quark matter and place important constraints on the stability and early evolution of protoquark stars, whose EOS differs

fundamentally from that of hadronic stars.

Comparing the temperatures obtained from QM [28] and hadronic EOSs at fixed s_B , we find that hadronic matter [57] systematically attains higher temperatures. This difference originates from the larger effective degeneracy of quark matter, which includes color and spin degrees of freedom [61], whereas typical hadronic models account primarily for spin degeneracy [58]. For a fixed thermodynamic state, the increased number of degrees of freedom in quark matter distributes the thermal energy among more microscopic modes, resulting in a lower temperature. In the present model, the temperature difference can reach up to $\sim 40\%$, suggesting that thermal profiles of newly born compact stars may provide a potential observational discriminator between hadronic and QM compositions.

The variation of ν/ν_K with M for rotating protoquark stars in fig. 3 highlights how the microscopic physics of deconfined quark matter governs their rotational behavior across evolutionary stages. In the hot, lepton-rich phases, pressure from thermal quarks and trapped neutrinos softens the EOS [28, 56], reducing compactness and lowering the Keplerian frequency ν_K . As a result, ν/ν_K increases rapidly with mass, indicating that hot protoquark stars approach the mass-shedding limit at relatively low masses, especially for strongly oblate configurations ($r_p/r_e = 0.5$). This observation is qualitatively similar to what is observed in rotating protoquark stars from hadronic EOS [47], for a general overview of relativistic rotating stars, see Ref. [62].

As the star cools and deleptonizes, thermal support is lost, and the zero-temperature QM EOS dominates, stiffened by Pauli blocking and repulsive vector interactions [63]. This increases compactness, raises both the maximum mass and ν_K [14], and allows cold quark stars to rotate at higher absolute frequencies while remaining farther from the mass-shedding limit. Rotation amplifies these trends through centrifugal flattening: hot quark matter is more susceptible to mass shedding, whereas cold, stiff quark matter sustains rapid rotation over a wider mass range. Together, these trends encode how quark-level thermodynamics translate into macroscopic rotational stability, offering a potential observational signature to distinguish quark stars from hadronic ones [5, 64].

Figure 4 shows that the moment of inertia (I) of rotating protoquark stars increases monotonically with M and is strongly enhanced by rotation, as decreasing r_p/r_e redistributes matter outward and raises I , with the most oblate configurations approaching the Keplerian limit [14, 70]. In panel $T = 0$, we have overlaid error bars representing the inferred observational constraints from the following pulsars: Red: J0437-4715, Blue: J0751+1807, Green: J1713+0747, Orange: J1802-2124, Purple: J1807-2500B, Brown: J1909-3744, Pink: J2222-0137, Gray: J0740+6620 (NICER), [65] Olive: J0030+0451 (NICER), [66] Cyan: J0737-3039A (Double Pulsar) [67-69]. Thermal evolution shifts the $I(M)$ sequences systematically: hot, lepton-rich stages yield the largest I due to a softened QM EOS and larger radii, while deleptonization stiffens the EOS, contracts the star, and reduces I

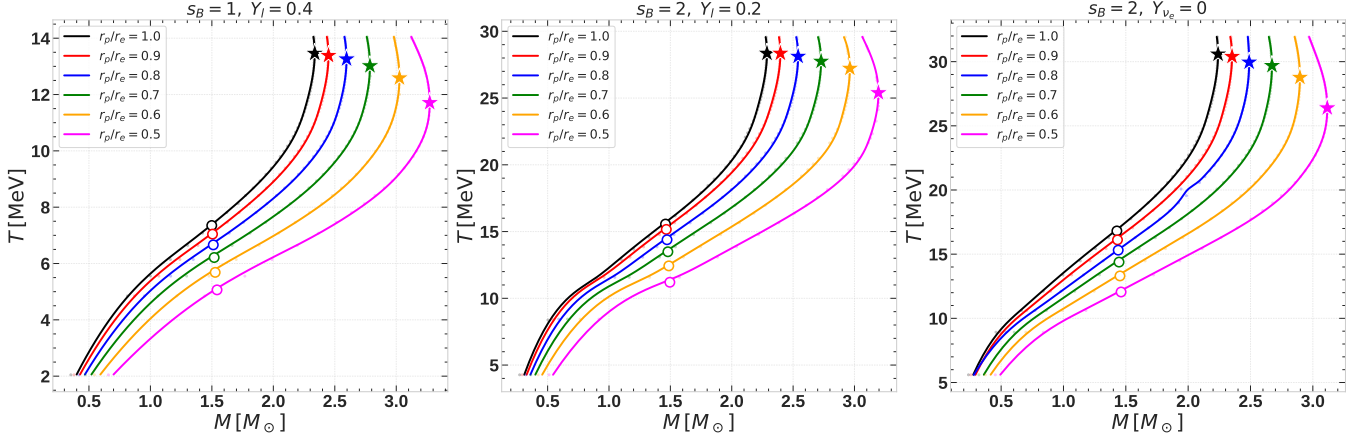


FIG. 2. The core temperature evolution of rotating proto stars examined along gravitational-mass sequences. The stars in the plots indicate the maximum mass for each configuration. The small open circles in the curve show the structural evolution of a single star with fixed baryonic mass of $1.55 M_{\odot}$.

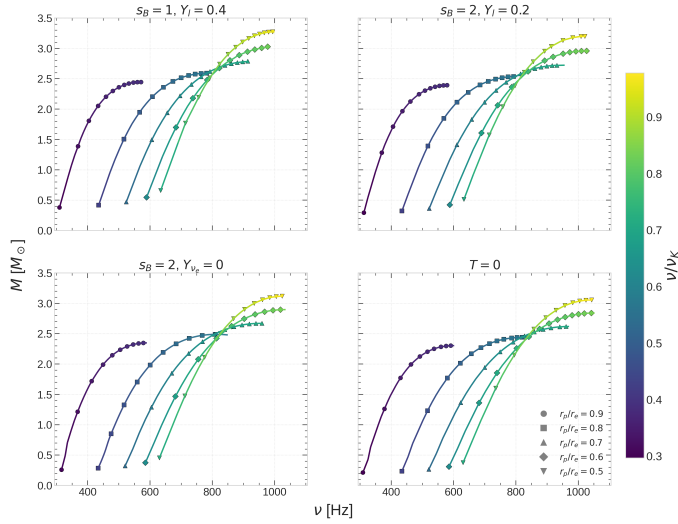


FIG. 3. Variation of the ratio of the rotational frequency to the Keplerian frequency ν/ν_K as a function of the stellar mass.

toward the cold, catalyzed limit. These trends encode the temperature and density-dependent strong interactions in quark matter and show that robust EOS constraints from I measurements must incorporate both rotational deformation and thermal history, with combined M - R - I data to provide a powerful discriminator between quark and hadronic interiors.

Protoquark stars and hadronic protoneutron stars exhibit qualitatively distinct I behavior due to their contrasting EOS. Although I increases with mass and rotation in both cases, hadronic matter remains stiffer at high density, yielding more compact stars with smaller radii and systematically lower I at fixed mass and flattening [71]. During deleptonization, hadronic stars may undergo a temporary stiffening that produces non-monotonic $I(M)$, (this non-monotonic behavior with thermodynamic conditions can be seen in Fig. 4 of [47]) whereas quark matter

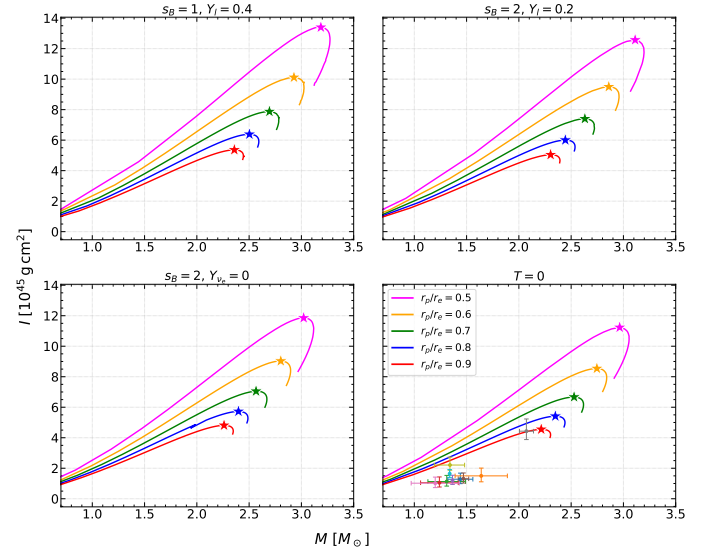


FIG. 4. The moment of inertia I as a function of the stellar mass for different rotational flattening. Overlaid error bars in panel $T = 0$ represent observational constraints from the following pulsars: Red: J0437–4715, Blue: J0751+1807, Green: J1713+0747, Orange: J1802–2124, Purple: J1807–2500B, Brown: J1909–3744, Pink: J2222–0137, Gray: J0740+6620 (NICER), [65] Olive: J0030+0451 (NICER), [66] Cyan: J0737–3039A (Double Pulsar) [67–69]. The I increases along the stable mass sequence up to M_{\max} (starred points along the curve) and then decreases as the mass decreases along the unstable branch.

softens in hot, lepton-rich stages, leading to larger radii and moments of inertia that can be 20–40% higher for the same mass and spin. Consequently, combined mass–radius–moment-of-inertia measurements provide a promising discriminator between hadronic and quark interiors [57, 58, 64].

Figure 5 shows that the angular momentum J of rotating protoquark stars increases monotonically with gravita-

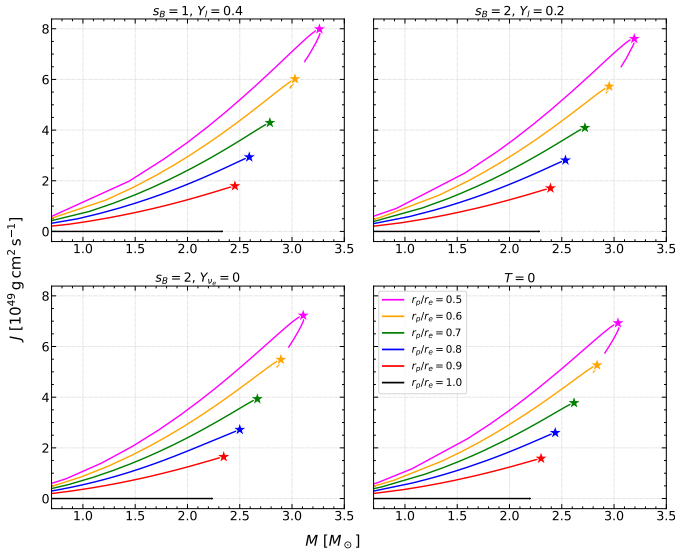


FIG. 5. Variation of the angular momentum, J , as a function of the stellar mass for different rotational flattening.

tional mass M and rises strongly with rotation, quantified by the decrease of r_p/r_e . Generally, hot, lepton-rich configurations store significantly more angular momentum than the lepton-poor ones [47] because thermal and neutrino pressures stiffen the QM EOS enhancing its maximum stellar mass, and increasing the moment of inertia (see the discussion in figs. 1 and 4). As the star deleptonizes, the EOS stiffens, the star contracts, and the $J(M)$ curves shift downward, with the cold, catalyzed sequences being the most compact. The most oblate configurations ($r_p/r_e \simeq 0.5$) approach the Keplerian mass-shedding limit (see fig. 3), which sets an upper bound on the attainable angular momentum [41, 48]. Overall, the figure highlights that both thermal evolution and rotational deformation critically control the angular-momentum budget of protoquark stars, with newly born lepton-rich objects capable of storing substantially more rotational energy than their cold lepton-poor descendants.

Comparatively, hadronic protoneutron stars show a similar qualitative increase of angular momentum with mass and rotation, but their stiffer nuclear EOS makes them more compact and able to store less angular momentum than QM stars of equal mass at the same rotational frequency, especially in hot, lepton-rich phases [47, 64]. Moreover, during deleptonization, hadronic stars may undergo a temporary stiffening that produces a non-monotonic $J(M)$ evolution, absent in QM sequences (see the comparative discussion in fig. 3), so that combined mass-radius-moment-of-inertia measurements could discriminate between hadronic and quark interior [66, 72].

The $|Q|(M)$ sequences in fig. 6 show that the magnitude of the quadrupole moment ($|Q|$) of rotating protoquark stars increases monotonically with M and is strongly amplified by rotation, with smaller r_p/r_e producing the higher deformation through centrifugal flattening [43]. Thermal evolution shifts these curves systematically: hot, lepton-rich stars exhibit the largest $|Q|$ because a soft-

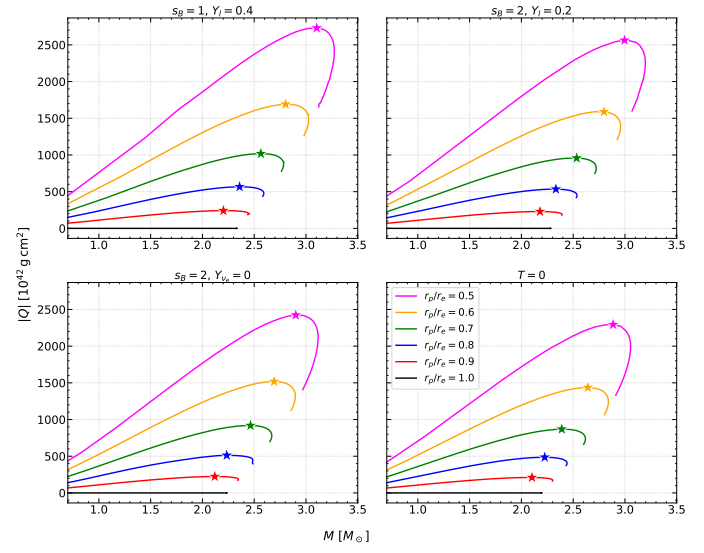


FIG. 6. Variation of the magnitude of the quadrupole moment $|Q|$ as a function of gravitational mass M for different rotational flattening.

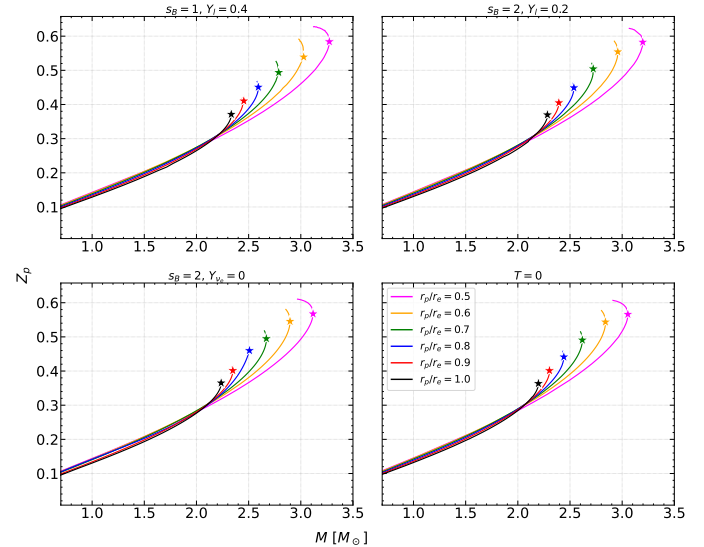


FIG. 7. Variation of the polar redshift Z_p against the gravitational mass for varying rotational flatness.

ened QM EOS and larger radii make them more easily deformable [28], while deleptonization stiffens the EOS, contracts the star, and reduces $|Q|$ toward the cold, catalyzed limit. This behavior reflects the temperature and density-dependent strong interactions in quark matter and has direct implications for gravitational-wave emission, as hot, rapidly rotating protoquark stars are stronger emitters whose signals weaken as the star cools [49, 73]. Compared to hadronic protoneutron stars, which are more compact and less deformable due to a stiffer high-density EOS, quark stars of the same mass and rotation develop larger quadrupole moments, especially in the early hot phases, making combined mass, radius, and quadrupole constraints a promising probe of the stellar

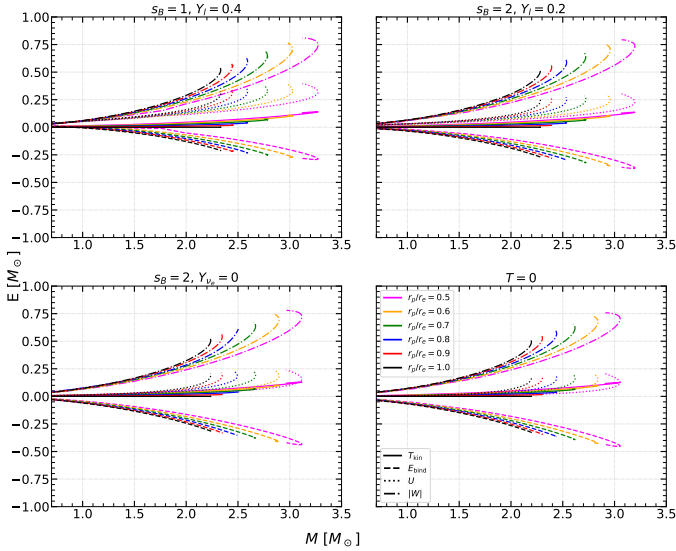


FIG. 8. The complete energy decomposition of rotating protoquark stars, including the gravitational potential energy $|W|$, rotational kinetic energy T_{kin} , binding energy E_{bind} , and internal energy, shown as functions of the gravitational mass.

interior [43, 64].

The polar redshift Z_p of rotating protoquark stars shown in fig. 7 increases monotonically with M at all evolutionary stages, reflecting the growth of stellar compactness [26, 41, 74]. Rotation systematically suppresses Z_p , as centrifugal support lowers the effective gravitational potential, with highly oblate configurations exhibiting the smallest redshifts at fixed mass [62]. Thermal evolution introduces a further ordering: hot, lepton-rich stars display the lowest Z_p because a softened QM EOS and larger radii reduce compactness, whereas cooling and deleptonization stiffen the EOS, contract the star, and shift the sequences upward toward the cold, catalyzed limit where Z_p is maximal. Hot, lepton-rich quark stars can exhibit significantly lower polar redshifts than hadronic stars of the same mass and rotation because their softer EOS leads to stronger thermal expansion [14, 57]. This implies that redshift measurements must be interpreted together with rotational state and thermal history, since a hot, rapidly rotating quark star can mimic a colder hadronic one; combined constraints on Z_p – M – R therefore offer a powerful probe of the dense-matter EOS [72].

Figure 8 shows how the gravitational potential energy $|W|$, rotational kinetic energy T_{kin} , binding energy E_{bind} , and internal energy U of rotating protoquark stars vary with M across their evolution from neutrino-trapped through deleptonization to cold, catalyzed states. All components grow in magnitude with mass: $|W|$ deepens as self-gravity strengthens [41], T_{kin} increases as more mass participates in rotation [48], E_{bind} becomes more negative, and U reflects the amount and thermal content of quark matter. Thermal evolution shifts the energy balance: at fixed rotation (r_p/r_e), hot, lepton-rich stars have larger internal energy U and a shallower $|W|$, while cooling and deleptonization reduce U and deepen $|W|$.

toward the cold, catalyzed limit [75]. Rotation further reshapes the balance: decreasing r_p/r_e enhances T_{kin} through centrifugal flattening, slightly reduces $|W|$, and weakens the binding, effects that are strongest near the Keplerian limit. These trends reflect the temperature and density-dependent strong interactions in quark matter and show how composition, thermal state, and spin jointly govern the energy budget and evolution of newly born compact stars. A first comprehensive energy decomposition of rotating quark stars was done in [29] for cold rotating quark stars.

Compared to hadronic matter, the softer QM EOS in hot, lepton-rich phases yields larger radii and lower compactness, leading to smaller gravitational binding $|W|$ and higher rotational kinetic energy T_{kin} at fixed mass and spin [64, 76]. By contrast, the stiffer nuclear EOS of hadronic stars produces more compact configurations with deeper gravitational potentials, resulting in larger $|W|$ and a reduced ability to store rotational energy, particularly at early times. By linking the star's mass, rotation, and thermal state to distinct energy partitions, this decomposition helps interpret observed spins, cooling rates, and stability limits of young compact stars. In particular, comparing inferred rotational energy, binding, and thermal content from timing, neutrino, or gravitational-wave data can help distinguish hot protoquark stars from hadronic ones and constrain the underlying EOS [77, 78].

IV. CONCLUSION

This work presents the first systematic investigation of rigidly rotating protoquark stars based on isentropic EOS within the DDQM framework. By constructing sequences of equilibrium configurations across four distinct evolutionary stages, from hot, lepton-rich matter to cold, catalyzed quark matter, we quantified the combined impact of thermal evolution and rotation on the global structure and key observables of these objects. Our results show that rotation substantially enhances the maximum stable mass, equatorial radius, angular momentum, moment of inertia, and quadrupole deformation, with mass increases reaching up to $\sim 40\%$ at the Keplerian limit (see the M_{max} in table I). The ratio of rotational kinetic to gravitational binding energy approaches $T_{\text{kin}}/|W| \simeq 0.18$ – 0.19 , indicating an increased susceptibility to non-axisymmetric instabilities and potential gravitational-wave emission. At fixed rotation, thermal evolution introduces systematic trends: as the stars cool and deleptonize, they become more compact and their global rotational quantities decrease (see figs. 1 to 7 and the results summary on table I).

The mass–radius relations demonstrate that hot protoquark stars are significantly larger than their cold counterparts, while rotation shifts the sequences to higher masses and radii. When both effects are included, a single QM EOS can accommodate current observational constraints from massive and large-radius compact stars (PSR J0740+6620) to a less massive supernova remnant HESS J1731–347 (see fig. 1). The thermal and rotational

analyses further reveal that softer EOS at early stages lead to lower Keplerian frequencies, whereas cooling and stiffening allow colder configurations to sustain faster absolute rotation. Distinctive trends emerge in key rotational observables. The moment of inertia, angular momentum, and quadrupole moment are strongly amplified in hot, rapidly rotating configurations, while the polar redshift is systematically reduced by centrifugal support and thermal expansion. The complete energy decomposition highlights how the balance between gravitational potential, internal, binding, and rotational energies evolves with both temperature and spin, providing complementary insight beyond standard bulk observables (see fig. 8).

Overall, our results demonstrate that the rotational properties of protoquark stars differ both qualitatively and quantitatively from those of hadronic protoneutron stars. These differences, encoded in the mass-radius relation, moment of inertia, quadrupole moment, and energy partitioning, offer a set of potential observational discriminants. Future multimessenger observations combining mass, radius, spin, and gravitational-wave information will be essential to test the QM hypothesis within the DDQM with temperature dependence. This work establishes a robust framework for future extensions, including differential rotation, magnetic fields, and dynamical sta-

bility studies of newly born compact stars.

ACKNOWLEDGMENTS

A. I. acknowledges financial support from the São Paulo State Research Foundation (FAPESP), Grant Nos. 2023/09545-1 and 2025/17347-0. This work is part of the project INCT-FNA (Proc. No. 464898/2014-5) and is also supported by the National Council for Scientific and Technological Development (CNPq) under Grants No. 306834/2022-7 (T.F.). T. F. also thanks the financial support from Improvement of Higher Education Personnel CAPES (Finance Code 001) and FAPESP Thematic Grants (2023/13749-1 and 2024/17816-8). P. Thakur is supported by the National Research Foundation of Korea (NRF) grant funded by the Korea government (MSIT) (No. RS-2024-00457037). This work was supported (in part) by the Yonsei University Research Fund (Yonsei University Frontier Fellowship for Postdoctoral Researchers) of 2025. A.K. acknowledges financial support from “The three-dimensional structure of the nucleon from lattice QCD” 3D-N-LQCD program, funded by the University of Cyprus, and from the projects HyperON (VISION ERC - PATH 2/0524/0001) and Baryon8 (POSTDOC/0524/0001), co-financed by the European Regional Development Fund and the Republic of Cyprus through the Research and Innovation Foundation.

[1] E. Witten, Cosmic Separation of Phases, *Phys. Rev. D* **30**, 272 (1984).

[2] C. Alcock, E. Farhi, and A. Olinto, Strange Stars, *Astrophys. J.* **310**, 261 (1986).

[3] A. R. Bodmer, Collapsed nuclei, *Phys. Rev. D* **4**, 1601 (1971).

[4] E. Farhi and R. L. Jaffe, *Phys. Rev. D* **30**, 2379 (1984).

[5] F. Weber, Strange quark matter and compact stars, *Prog. Part. Nucl. Phys.* **54**, 193 (2005), [arXiv:astro-ph/0407155](https://arxiv.org/abs/astro-ph/0407155).

[6] J. J. Drake *et al.*, Is RXJ1856.5-3754 a quark star?, *Astrophys. J.* **572**, 996 (2002), [arXiv:astro-ph/0204159](https://arxiv.org/abs/astro-ph/0204159).

[7] V. Doroshenko, V. Suleimanov, G. Pühlhofer, and A. Santangelo, A strangely light neutron star within a supernova remnant, *Nature Astronomy* **6**, 1444 (2022).

[8] X.-D. Li, S. Ray, J. Dey, M. Dey, and I. Bombaci, On the Nature of the compact star in 4u 1728-34, *Astrophys. J. Lett.* **527**, L51 (1999), [arXiv:astro-ph/9908274](https://arxiv.org/abs/astro-ph/9908274).

[9] F. Di Clemente, A. Drago, and G. Pagliara, Is the Compact Object Associated with HESS J1731-347 a Strange Quark Star? A Possible Astrophysical Scenario for Its Formation, *Astrophys. J.* **967**, 159 (2024), [arXiv:2211.07485 \[astro-ph.HE\]](https://arxiv.org/abs/2211.07485).

[10] J. M. Lattimer, M. Prakash, D. Masak, and A. Yahil, Rapidly Rotating Pulsars and the Equation of State, *Astrophys. J.* **355**, 241 (1990).

[11] N. Stergioulas, W. Kluźniak, and T. Bulik, Keplerian frequencies and innermost stable circular orbits of rapidly rotating strange stars, *Astronomy and Astrophysics* **352**, L116 (1999), [arXiv:astro-ph/9909152 \[astro-ph\]](https://arxiv.org/abs/astro-ph/9909152).

[12] J. L. Zdunik, T. Bulik, W. Kluźniak, P. Haensel, and D. Gondek-Rosińska, On the mass of moderately rotating strange stars in the mit bag model and lmxbs, *Astronomy and Astrophysics* **359**, 143 (2000), [arXiv:astro-ph/0004278 \[astro-ph\]](https://arxiv.org/abs/astro-ph/0004278).

[13] A. J. Romanowsky and C. S. Kochanek, Dynamics of stars and globular clusters in m87, *Astrophys. J.* **553**, 722 (2001), [arXiv:astro-ph/0008062](https://arxiv.org/abs/astro-ph/0008062).

[14] D. Gondek-Rosińska, T. Bulik, L. Zdunik, E. Gourgoulhon, S. Ray, J. Dey, and M. Dey, Rotating compact strange stars, *Astron. Astrophys.* **363**, 1005 (2000), [arXiv:astro-ph/0007004](https://arxiv.org/abs/astro-ph/0007004).

[15] J. L. Zdunik and P. Haensel, Maximum rotation frequency of strange stars, *Phys. Rev. D* **42**, 710 (1990).

[16] M. Prakash, E. Baron, and M. Prakash, Erratum: Rotation of stars containing strange quark matter [Phys. Lett. B 243 (1990) 175], *Phys. Lett. B* **247**, 632 (1990).

[17] D. Gondek-Rosińska, T. Bulik, J. L. Zdunik, E. Gourgoulhon, S. Ray, J. Dey, and M. Dey, Rapidly rotating compact strange stars, *Astronomy and Astrophysics* **363**, 1005 (2000), [arXiv:astro-ph/0007004 \[astro-ph\]](https://arxiv.org/abs/astro-ph/0007004).

[18] S. Bhattacharyya, I. Bombaci, D. Logoteta, and A. V. Thampan, Fast spinning strange stars: possible ways to constrain interacting quark matter parameters, *Mon. Not. Roy. Astron. Soc.* **457**, 3101 (2016), [arXiv:1601.06120 \[astro-ph.HE\]](https://arxiv.org/abs/1601.06120).

[19] E. Gourgoulhon, P. Haensel, R. Livine, E. Paluch, S. Bonazzola, and J. A. Marck, Fast rotation of strange stars, *Astron. Astrophys.* **349**, 851 (1999), [arXiv:astro-ph/9907225](https://arxiv.org/abs/astro-ph/9907225).

[20] E. Zhou, A. Tsokaros, L. Rezzolla, and R. Xu, Maxi-

mum mass of axisymmetric rotating quark stars, *Astron. Nachrichten* **338**, 1044 (2017).

[21] M. Szkudlarek, D. Gondek-Rosińska, L. Villain, and M. Ansorg, The Maximum Mass of Rotating Strange Stars, in *Electromagnetic Radiation from Pulsars and Magnetars*, Astronomical Society of the Pacific Conference Series, Vol. 466, edited by W. Lewandowski, O. Maron, and J. Kijak (2012) p. 231.

[22] M. Szkudlarek, D. Gondek-Rosińska, L. Villain, and M. Ansorg, Maximum Mass Of Differentially Rotating Strange Quark Stars, *Astrophys. J.* **879**, 44 (2019), arXiv:1904.03759 [astro-ph.HE].

[23] E. Zhou, A. Tsokaros, K. Uryu, R. Xu, and M. Shibata, Differentially rotating strange star in general relativity, *Phys. Rev. D* **100**, 043015 (2019), arXiv:1902.09361 [astro-ph.HE].

[24] E. Zhou, Properties of relativistically rotating quark stars, in *Journal of Physics Conference Series*, Journal of Physics Conference Series, Vol. 861 (2017) p. 012007.

[25] E. Zhou, A. Tsokaros, L. Rezzolla, R. Xu, and K. Uryu, Uniformly rotating, axisymmetric, and triaxial quark stars in general relativity, *Phys. Rev. D* **97**, 023013 (2018).

[26] N. Stergioulas and J. L. Friedman, Comparing Models of Rapidly Rotating Relativistic Stars Constructed by Two Numerical Methods, *Astrophys. J.* **444**, 306 (1995), arXiv:astro-ph/9411032 [astro-ph].

[27] F. M. da Silva, A. Issifu, L. L. Lopes, L. C. N. Santos, and D. P. Menezes, Bayesian study of quark models in view of recent astrophysical constraints, *Phys. Rev. D* **109**, 043054 (2024), arXiv:2309.16865 [nucl-th].

[28] A. Issifu, F. M. da Silva, and D. P. Menezes, Proto-strange quark stars from density-dependent quark mass model, *Eur. Phys. J. C* **84**, 463 (2024), arXiv:2311.12511 [nucl-th].

[29] A. Issifu, A. Konstantinou, F. M. da Silva, and T. Frederico, Rotational effects in quark stars: comparing different models (2025), arXiv:2511.20477 [astro-ph.HE].

[30] J.-y. Shen, Y. Zhang, B. Wang, and R.-K. Su, Slowly rotating proto strange stars in quark mass density- and temperature- dependent model, *Int. J. Mod. Phys. A* **20**, 7547 (2005), arXiv:gr-qc/0503015.

[31] J. Madsen, Physics and astrophysics of strange quark matter, *Lect. Notes Phys.* **516**, 162 (1999), arXiv:astro-ph/9809032.

[32] K. Chen and L.-M. Lin, Fully general relativistic simulations of rapidly rotating quark stars: Oscillation modes and universal relations, *Phys. Rev. D* **108**, 064007 (2023), arXiv:2307.01598 [gr-qc].

[33] C. J. Xia, G. X. Peng, S. W. Chen, Z. Y. Lu, and J. F. Xu, Thermodynamic consistency, quark mass scaling, and properties of strange matter, *Phys. Rev. D* **89**, 105027 (2014), arXiv:1405.3037 [hep-ph].

[34] A. Issifu, F. M. da Silva, L. C. N. Santos, D. P. Menezes, and T. Frederico, Strongly interacting quark matter in massive quark stars, *Classical and Quantum Gravity* **42**, 125004 (2025).

[35] X. J. Wen, X. H. Zhong, G. X. Peng, P. N. Shen, and P. Z. Ning, Thermodynamics with density and temperature dependent particle masses and properties of bulk strange quark matter and strangelets, *Phys. Rev. C* **72**, 015204 (2005), arXiv:hep-ph/0506050.

[36] G. X. Peng, H. C. Chiang, and P. Z. Ning, Thermodynamics, strange quark matter, and strange stars, *Phys. Rev. C* **62**, 025801 (2000), arXiv:hep-ph/0003027.

[37] B. C. Backes, E. Hafemann, I. Marzola, and D. P. Menezes, Density dependent quark mass model revisited: Thermodynamic consistency, stability windows and stellar properties, *J. Phys. G* **48**, 055104 (2021), arXiv:2007.04494 [hep-ph].

[38] A. Deur, S. J. Brodsky, and G. F. de Teramond, The QCD Running Coupling, *Nucl. Phys.* **90**, 1 (2016), arXiv:1604.08082 [hep-ph].

[39] R. L. Workman *et al.* (Particle Data Group), Review of Particle Physics, *PTEP* **2022**, 083C01 (2022).

[40] H.-M. Chen, C.-J. Xia, and G.-X. Peng, Strangelets at finite temperature in a baryon density-dependent quark mass model, *Phys. Rev. D* **105**, 014011 (2022), arXiv:2110.09194 [hep-ph].

[41] G. B. Cook, S. L. Shapiro, and S. A. Teukolsky, Rapidly Rotating Neutron Stars in General Relativity: Realistic Equations of State, *Astrophys. J.* **424**, 823 (1994).

[42] H. Komatsu, Y. Eriguchi, and I. Hachisu, Rapidly rotating general relativistic stars. i – numerical method and its application to uniformly rotating polytropes, *Mon. Not. R. Astron. Soc.* **237**, 355 (1989).

[43] W. G. Laarakkers and E. Poisson, Quadrupole moments of rotating neutron stars, *Astrophys. J.* **512**, 282 (1999), arXiv:gr-qc/9709033.

[44] G. Pappas and T. A. Apostolatos, *Multipole moments of numerical spacetimes* (2012), arXiv:1211.6299 [gr-qc].

[45] A. Konstantinou and S. M. Morsink, Universal relations for the increase in the mass and radius of a rotating neutron star, *The Astrophysical Journal* **934**, 139 (2022).

[46] A. Konstantinou, The effect of a self-bound equation of state on the structure of rotating compact stars, *The Astrophysical Journal* **997**, 55 (2026).

[47] F. M. da Silva, A. Issifu, L. C. N. Santos, T. Frederico, and D. P. Menezes, Hyperons and Δ 's in rotating protoneutron stars: Global properties, *Phys. Rev. D* **112**, 023007 (2025), arXiv:2504.05495 [hep-ph].

[48] N. Stergioulas, Rotating Stars in Relativity, *Living Rev. Rel.* **6**, 3 (2003), arXiv:gr-qc/0302034.

[49] N. Andersson, Gravitational waves from instabilities in relativistic stars, *Class. Quant. Grav.* **20**, R105 (2003), arXiv:astro-ph/0211057.

[50] D. Gondek-Rosińska, N. Stergioulas, T. Bulik, W. Kluzniak, and E. Gourgoulhon, Lower limits on the maximum orbital frequency around rotating strange stars, *Astron. Astrophys.* **380**, 190 (2001), arXiv:astro-ph/0110209.

[51] T. Riley *et al.*, A *NICER* View of PSR J0030+0451: Millisecond Pulsar Parameter Estimation, *Astrophys. J. Lett.* **887**, L21 (2019).

[52] M. Miller *et al.*, PSR J0030+0451 Mass and Radius from *NICER* Data and Implications for the Properties of Neutron Star Matter, *Astrophys. J. Lett.* **887**, L24 (2019), arXiv:1912.05705 [astro-ph.HE].

[53] T. E. Riley *et al.*, A nicer view of the massive pulsar psr j0740+6620 informed by radio timing and xmm-newton spectroscopy, *Astrophys. J. Lett.* **918** (2021).

[54] M. C. Miller *et al.*, The Radius of PSR J0740+6620 from NICER and XMM-Newton Data, *Astrophys. J. Lett.* **918**, L28 (2021), arXiv:2105.06979 [astro-ph.HE].

[55] D. Choudhury *et al.*, A NICER View of the Nearest and Brightest Millisecond Pulsar: PSR J0437–4715, *Astrophys. J. Lett.* **971**, L20 (2024).

[56] M. Kumari and A. Kumar, Properties of strange quark matter and strange quark stars, *Eur. Phys. J. C* **81**, 791 (2021).

[57] J. A. Pons, S. Reddy, M. Prakash, J. M. Lattimer, and J. A. Miralles, Evolution of protoneutron stars, *Astrophys.*

J. **513**, 780 (1999), arXiv:astro-ph/9807040.

[58] M. Prakash, I. Bombaci, M. Prakash, P. J. Ellis, J. M. Lattimer, and R. Knorren, Composition and structure of protoneutron stars, *Phys. Rept.* **280**, 1 (1997), arXiv:nucl-th/9603042.

[59] A. Issifu, K. D. Marquez, M. R. Pelicer, and D. P. Menezes, Exotic baryons in hot neutron stars, *Mon. Not. Roy. Astron. Soc.* **522**, 3263 (2023), arXiv:2302.04364 [nucl-th].

[60] J. E. Horvath, L. S. Rocha, L. M. de Sá, P. H. R. S. Moraes, L. G. Barão, M. G. B. de Avellar, A. Bernardo, and R. R. A. Bachega, A light strange star in the remnant HESS J1731–347: Minimal consistency checks, *Astron. Astrophys.* **672**, L11 (2023), arXiv:2303.10264 [astro-ph.HE].

[61] G. Lugones and J. E. Horvath, High-density QCD pairing in compact star structure, *Astron. Astrophys.* **403**, 173 (2003), arXiv:astro-ph/0211638.

[62] V. Paschalidis and N. Stergioulas, Rotating Stars in Relativity, *Living Rev. Rel.* **20**, 7 (2017), arXiv:1612.03050 [astro-ph.HE].

[63] M. Alföldi, P. Jotwani, C. Kouvaris, J. Kundu, and K. Rajagopal, A Hot water bottle for aging neutron stars, *Phys. Rev. D* **71**, 114011 (2005), arXiv:astro-ph/0411560.

[64] M. Oertel, M. Hempel, T. Klähn, and S. Typel, Equations of state for supernovae and compact stars, *Rev. Mod. Phys.* **89**, 015007 (2017), arXiv:1610.03361 [astro-ph.HE].

[65] Y. Li, J. Wang, Z. Wu, and D. Wen, Inferring the gravitational binding energy and moment of inertia of psr j0030 + 0451 and psr j0740 + 6620 from new universal relations, *Classical and Quantum Gravity* **39**, 035014 (2022).

[66] H. O. Silva, A. M. Holgado, A. Cárdenas-Avendaño, and N. Yunes, Astrophysical and theoretical physics implications from multimessenger neutron star observations, *Phys. Rev. Lett.* **126**, 181101 (2021), arXiv:2004.01253 [gr-qc].

[67] B. Kumar and P. Landry, Inferring neutron star properties from GW170817 with universal relations, *Phys. Rev. D* **99**, 123026 (2019), arXiv:1902.04557 [gr-qc].

[68] S. Yang, D. Wen, J. Wang, and J. Zhang, Exploring the universal relations with the correlation analysis of neutron star properties, *Phys. Rev. D* **105**, 063023 (2022).

[69] M. Bejger, T. Bulik, and P. Haensel, Moments of inertia of the binary pulsars J0737-3039A,B and the dense matter EOS, *Mon. Not. Roy. Astron. Soc.* **364**, 635 (2005), arXiv:astro-ph/0508105.

[70] C. Breu and L. Rezzolla, Maximum mass, moment of inertia and compactness of relativistic stars, *Mon. Not. Roy. Astron. Soc.* **459**, 646 (2016), arXiv:1601.06083 [gr-qc].

[71] D. G. Ravenhall and C. J. Pethick, Neutron Star Moments of Inertia, *Astrophys. J.* **424**, 846 (1994).

[72] K. Yagi and N. Yunes, Approximate Universal Relations for Neutron Stars and Quark Stars, *Phys. Rept.* **681**, 1 (2017), arXiv:1608.02582 [gr-qc].

[73] C. Cutler, Gravitational waves from neutron stars with large toroidal B fields, *Phys. Rev. D* **66**, 084025 (2002), arXiv:gr-qc/0206051.

[74] J. M. Lattimer and M. Prakash, Neutron star structure and the equation of state, *Astrophys. J.* **550**, 426 (2001), arXiv:astro-ph/0002232.

[75] A. Burrows and J. M. Lattimer, The birth of neutron stars, *Astrophys. J.* **307**, 178 (1986).

[76] N. Glendenning, *Compact Stars. Nuclear Physics, Particle Physics and General Relativity*. (1996).

[77] J. M. Lattimer and M. Prakash, The physics of neutron stars, *Science* **304**, 536 (2004), arXiv:astro-ph/0405262.

[78] C. M. Will, Testing general relativity with compact-body orbits: a modified Einstein–Infeld–Hoffmann framework, *Class. Quant. Grav.* **35**, 085001 (2018), arXiv:1801.08999 [gr-qc].